Current Opinion in Colloid & Interface Science 16 (2011) 517–524

Contents lists available at ScienceDirect

Current Opinion in Colloid & Interface Science

journal homepage: www.elsevier.com/locate/cocis

Hydration force due to the reduced screening of the electrostatic repulsion in few-nanometer-thick films

Peter A. Kralchevsky *, Krassimir D. Danov, Elka S. Basheva

Department of Chemical Engineering, Faculty of Chemistry, Sofia University, 1164 Sofia, Bulgaria

ARTICLE INFO

Article history:
Received 24 March 2011
Received in revised form 21 April 2011
Accepted 22 April 2011
Available online 4 May 2011

Keywords:
Surface forces
Hydration repulsion
Foam films
Effect of counterion size

ABSTRACT

Experiments with foam films from solutions of 1 mM SDS + 100 mM electrolyte (LiCl, NaCl and CsCl) were carried out by a thin-film-pressure balance. The measured dependences of disjoining pressure versus film thickness exhibit a steep increase when the thickness of the film's water core becomes smaller than 3.7 nm. This behavior can be interpreted as a manifestation of the hydration force. We unsuccessfully tried to interpret the data with different available theoretical models. Eventually, we found that a relatively simple model of "reduced screening" can fit the data. Such reduced screening of the electric field could exist only in a narrow range of film thicknesses, which practically coincides with the region where the hydration repulsion is acting. This model and its experimental verification are described in the article.

1. Introduction

The existence of a "hydration" layer was proposed as a possible explanation for the stability of hydrophilic colloids, even when the particles are uncharged [1]. The existence of a short range (≤4 nm) repulsive pressure was observed in experiments on the swelling of clays [2,3] and on the stabilization of foam films [4]. This short-range repulsion has been called the "hydration force" [5]. The Derjaguin's school terms it "structural component of disjoining pressure" [6]. Indications for its action were found in measurements of interactions between phospholipid bilayers by Parsegian, Rand et al. [7,8]. Israelachvili et al. [9–11] and Pashley [12–14] examined the validity of the Derjaguin–Landau–Verwey–Overbeek (DLVO) theory [15,16] at small film thickness by a surface-force apparatus in experiments with films from aqueous electrolyte solutions confined between two curved mica surfaces, bare or covered by adsorbed layers. At electrolyte concentrations below 10^{-4} M, they observed the typical DLVO maximum. However, at electrolyte concentrations higher than 10^{-3} M they did not observe the expected DLVO maximum and primary minimum [11]. Instead a strong short-range repulsion was detected, which can be empirically described by exponential law with a decay length 0.6–1.1 nm [17]. Similar repulsion was detected between silica sheets [18,19] and dihexadecyl phosphate monolayers deposited on a solid surface [20].

As known, the conventional electrostatic (double layer) repulsion is suppressed if the solution's ionic strength is increased [15,16]. In contrast, the hydration repulsion is detected at higher ionic strengths [11], at which it is the main stabilizing factor in liquid films and colloidal dispersions. Such strong repulsion at high salt concentrations was observed between apoferritin molecules in solutions [21,22] and between the adsorption layers of this protein on silica surfaces [23]. In general, the hydration force plays an important role for the stability of proteins in physiological media. Effects of monovalent anions of the Hofmeister series on the hydration repulsion between lipid bilayers have been experimentally investigated [24,25]. The hydration repulsion affects the stability of emulsions [26]; the rheology of concentrated suspensions [27]; the interactions of biological cells [28], and the fusion rate of vesicles in the cellular inter-organelle traffic [29]. Additional information can be found in the review articles [30–34].

Different models have been proposed for theoretical explanation of the hydration repulsion. In the water-structuring models, the short-range repulsive interaction is attributed to an alignment of water dipoles in the vicinity of a hydrophilic surface, where the range of the surface force is determined by the orientation-correlation length of the solvent molecules [35–37].

The image-charge models take into account the discreteness of the surface charges, which induce orientation in the adjacent water dipoles [38–41]. Dipoles due to zwitterionic surface groups, e.g. phospholipid headgroups [42], have been also taken into consideration in models of the electrostatic interaction between planar lattices of dipoles [43–47].

The dielectric-saturation models attribute the hydration repulsion to the presence of a layer with lower dielectric constant, ε, in the vicinity of the interfaces. Models with a stepwise [48,49] and continuous [50] variation of ε have been proposed.

* Corresponding author. Tel.: +359 2 8161262; fax: +359 2 9625643.
E-mail address: pk@lcpe.uni-sofia.bg (P.A. Kralchevsky).

1359-0294/$ – see front matter © 2011 Elsevier Ltd. All rights reserved.
doi:10.1016/j.cocis.2011.04.005

The excluded-volume model [51,52] takes into account the fact that the finite size of the ions leads to a lower counterion concentration near a charged surface, and to a weaker Debye screening of the electrostatic field (in comparison with the point-ion model), which results in a stronger repulsion between two charged surfaces at short separations.

Israelachvili and Wennerström [53] demonstrated that effects of different physical origin are termed "hydration repulsion". For example, the short-range repulsion between lipid membranes can be a manifestation of undulation, peristaltic and protrusion forces, which are due to thermally excited fluctuations at the interfaces [53]. For the time being, the current opinion of the researchers in the field colloid science is that despite the proposed explanations, the origin of hydration repulsion remains unclear [54].

Here, we make an additional attempt to clarify the physical origin of the short-range repulsion between two charged surfaces at higher electrolyte concentrations. For this goal, we first obtained a set of data for the dependence of disjoining pressure on the thickness of foam films stabilized by an anionic surfactant (Section 2). To check the effect of counterion size, three different electrolytes were used: LiCl, NaCl and CsCl, each of them at a concentration of 0.1 M. At larger film thicknesses, the data are in excellent agreement with the DLVO theory, whereas at smaller (few nanometer) thicknesses a strong short-range repulsion is observed, which significantly deviates from the DLVO predictions. The comparison of theory and experiment shows that the excluded volume model [51,52] predicts a repulsive force that is much weaker than the experimentally observed one. The analysis of the results led us to the formulation of a new model, which is presented in Section 3 and tested against the experimental data in Section 4.

2. Experimental investigation of hydration force in foam films

The foam films were formed from 1 mM solutions of sodium dodecyl sulfate (SDS), Across, 99% pure. As mentioned above, the used electrolytes were LiCl, NaCl and CsCl, products of Sigma (>99% pure). The addition of KCl and RbCl leads to precipitation of the SDS solutions. For this reason, the latter salts were not used in the experiments. All solutions were prepared with deionized water of specific resistivity 18.2 MΩ·cm (Milli-Q purification system). The working temperature was 25 °C.

The dependence of disjoining pressure, Π, versus the film thickness, h_t, was measured by means of a Mysels–Jones (MJ) experimental cell [55], which is also termed "thin film pressure balance" [56]. The film is formed in the center of a cylindrical hole in a porous-glass plate and allows forcing the two film surfaces against each other at pressures up to 7000 Pa in our experiments. The film thickness is determined by an interference method [57,58] from the intensity of the monochromatic light (546 nm) reflected from the film. The reflected light is supplied to a photomultiplier and computer, and the film thickness is recorded continuously during the experiment. The applied pressure is measured electronically, by a pressure transducer. A detailed description of the used MJ-cell version can be found elsewhere [59].

During the experiment, the applied pressure was increased in small steps, of 40 Pa for Π<3000 Pa, and of 100 Pa for Π>3000 Pa. After each pressure increase, the computer's indications for the film thickness are observed (for about 10 min) until an equilibrium thickness is established, which is recorded together with the respective value of pressure. After that, the pressure is increased again to obtain the next experimental point.

Experimental $\Pi(h_t)$ curves obtained in the presence of LiCl, NaCl and CsCl are shown in Fig. 1a. The order of the curves corresponds to the size of the counterions: the strength of the measured repulsion increases in the order $Cs^+ < Na^+ < Li^+$. The right-hand-side branch of each experimental curve is in excellent agreement with the prediction

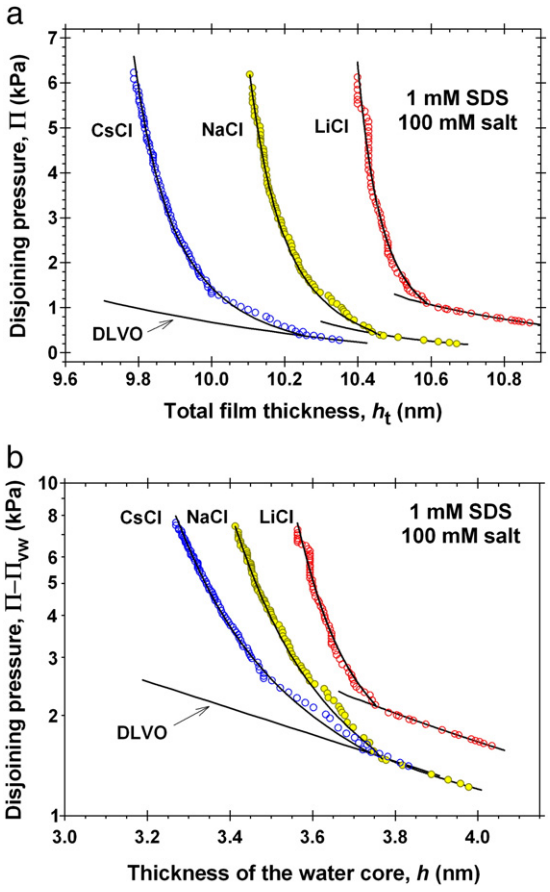

Fig. 1. (a) Experimental data for the disjoining pressure Π vs. the thickness h_t of foam films formed from 1 mM SDS solutions that contain 100 mM salt: LiCl, NaCl or CsCl. The lower branch of each experimental curve is in agreement with the DLVO theory, whose prediction is shown by a solid line. The upper branch corresponds to hydration repulsion, and the respective theoretical curve is drawn in accordance with the reduced-screening model; see Eqs. (14) and (23). (b) The same data plotted as $\Pi_{el} \equiv \Pi - \Pi_{vw}$ vs. the thickness of the film's water core, h, in semi-logarithmic scale; Π_{el} and Π_{vw} are, respectively, the electrostatic and van der Waals components of disjoining pressure.

of the DLVO theory, which is shown by solid line in Fig. 1a; see Eqs. (6), (8) and Section 4.2 below. Conversely, the left-hand-side branch of each curve corresponds to Π-values that are much greater than the DLVO predictions. The latter branch can be considered as a manifestation of the short-range hydration force.

Fig. 1b shows the electrostatic component of disjoining pressure, $\Pi_{el} \equiv \Pi - \Pi_{vw}$, plotted vs. the thickness of the film's water core, h, in semi-logarithmic scale; see Section 4.1 for the calculation of h. The van der Waals component of disjoining pressure is calculated from the known formula $\Pi_{vw} = -A_H/(6\pi h_t)$, where A_H is the Hamaker parameter. The slopes of the DLVO branches of the experimental curves correspond to $\kappa^{-1} = 1.08$, 1.09 and 0.90 nm (with errors ≤0.1 nm), respectively, for LiCl, NaCl and CsCl. The latter values are close to the value of the Debye length, which is $\kappa^{-1} = 0.96$ nm for a solution of ionic strength 100 mM. The "hydration" branches of the experimental curves considerably deviate from straight lines in semi-logarithmic scale. In other words, the data indicate that the hydration force does not obey a simple exponential law. A similar result was obtained by Pashley [14], who established (in experiments by a surface-force apparatus) that the hydration repulsion can be described by a double-exponential decay. A model, which provides a quantitative explanation of the experimental dependencies, is proposed in Section 3.2.

3. Theoretical models

3.1. Comparison with the ionic-excluded-volume model

As already mentioned, we tried to fit the experimental $\Pi(h_t)$ curves in Fig. 1 by means of the excluded-volume model that takes into account the finite size of the hydrated ions in the solution. Because the effect of dielectric saturation was found to be small [51], we used the "purely-excluded-volume" version of the model from Ref. [52]. First, this model was applied to fit the lower (right-hand-side) branch of each experimental curve, which turns out to correspond to a fixed potential. From the respective fit, the value of the surface electrostatic potential was determined, which was further applied to compute the whole theoretical curve. To our surprise, under the conditions of our experiment, the theoretical curves computed by the excluded-volume model [52] practically coincide with the predictions of the DLVO theory shown in Fig. 1, i.e. this model cannot explain the "hydration" branches of the data. The curves predicted by the two models ("excluded volume" and DLVO) are so close that they cannot be distinguished in the scale of Fig. 1. The distinct difference between the two models presented in Fig. 4b of Ref. [52] corresponds to film thicknesses that are considerably smaller than those of the water core in our experiments, and to pressure values that are by many orders of magnitude higher than those registered in our experiments (Fig. 1). It is possible to fit the whole experimental curves (including the "hydration" branch) by the "excluded volume" model if we assume that the surface electric potential strongly increases with the decrease of the film thickness, which is rather unlikely.

3.2. Reduced-screening (RS) model

To explain the powerful repulsion observed at small distances, here we propose a new model that takes into account the fact that in nanometer-thick films the free ions are unable to screen the electric field of the film surfaces as effectively as they are doing that at larger thicknesses. The idea is illustrated in Fig. 2.

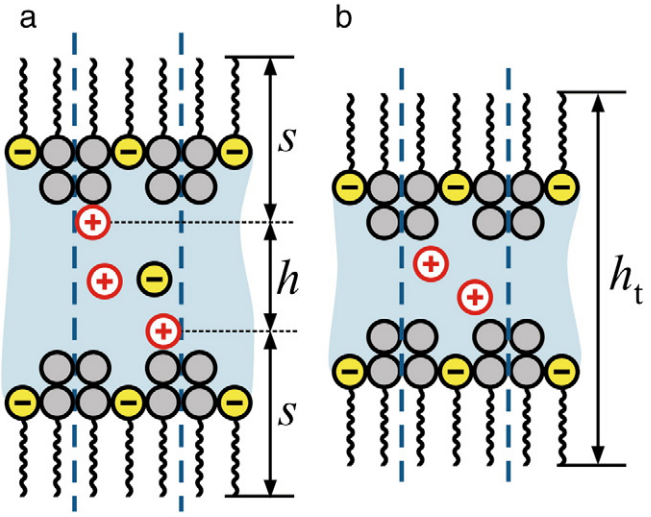

Fig. 2. Sketch of a foam film stabilized by anionic surfactant. A part of the adsorbed surfactant ions (shown in gray color) are neutralized by bound counterions. (a) At larger thicknesses, the electrostatic repulsion is screened by both counterions dissociated from the film surfaces and ions from the dissolved electrolyte (Debye screening). (b) At sufficiently small thicknesses (in few-nanometer-thick films), only counterions dissociated from the surfaces remain in the film which leads to a *reduced screening* of the electrostatic field and to a stronger repulsion between the film surfaces. s is the thickness of the adsorption layer at the film surface; h is the thickness of the water core, and $h_t = h + 2s$ is the total film thickness.

Let us consider a part of the film (a cell) that contains one electric charge on each of the two film surfaces. In Fig. 2, this cell is confined between the two vertical dashed lines. In average, such a cell must be *electroneutral*. Hence, it can contain the two counterions of the ionized surface groups, as well as an integer number of dissociated molecules from the added electrolyte. (In Fig. 2a, one such dissociated molecule is shown.) If the distance between the two film surfaces is diminishing, the number of dissociated electrolyte molecules in the cell will diminish because of the restricted space, until eventually only the two counterions dissociated from the ionized surface groups remain in the cell, as shown in Fig. 2b. The transition from the situation in Fig. 2a to that in Fig. 2b is accompanied with a significant weakening in the screening of the electrostatic field, as demonstrated below on the basis of the Poisson–Boltzmann equation.

First, let us numerate the ionic components present in the considered system: 1 — surfactant ion (like the dodecyl-sulfate anion); 2 — counterion (like Li^+, Na^+ or Cs^+), and 3 — co-ion from the salt (like Cl^-). At the higher electrolyte concentrations, at which the hydration repulsion is observed, the Boltzmann equation is accurate in terms of activities [60]:

$$a_1 = a_{1\infty}e^{-\Phi}, \qquad a_2 = a_{2\infty}e^{\Phi}, \qquad a_3 = a_{3\infty}e^{-\Phi} \tag{1}$$

where a_i is the local activities of the respective ion ($i = 1, 2, 3$); $a_{i\infty} = c_{i\infty}\gamma_{\pm}$, where $a_{i\infty}$ is the bulk activity; $c_{i\infty}$ is the bulk concentration and $\gamma_{\pm}$ is the bulk activity coefficient; Φ is the dimensionless electrostatic potential:

$$\Phi \equiv \frac{e|\psi|}{kT} \tag{2}$$

T is the temperature; k is the Boltzmann constant; e is the electronic charge, and ψ is the dimensional potential. Φ defined by Eq. (2) is non-negative; as usual $\Phi = 0$ in the bulk of solution. The Boltzmann distributions in Eq. (1) are equivalent to the condition for uniformity of the electrochemical potential of the respective ions throughout the electric double layer [60].

In view of Eqs. (1) and (2), for the film of greater thickness (Fig. 2a) the Poisson–Boltzmann equation can be presented in the form:

$$\frac{d^2\Phi}{dx^2} = \frac{1}{2}\kappa^2\left(e^{\Phi} - e^{-\Phi}\right) \tag{3}$$

where we have used the relationship $a_{1\infty} + a_{3\infty} = a_{2\infty}$, which is a corollary from the bulk electroneutrality condition; x is the coordinate in direction normal to the film surfaces; κ is the Debye parameter in terms of activities:

$$\kappa^2 \equiv \frac{2e^2 a_{2\infty}}{\varepsilon\varepsilon_0 kT} \tag{4}$$

ε_0 is the dielectric permittivity of vacuum and ε is the dielectric constant of water. The Poisson–Boltzmann equation in terms of activities, Eq. (3), has been successfully applied for numerical interpretation of the surface-tension isotherms of numerous ionic surfactants at various salt concentrations [61–65]. Here, our goal is to compare the basic equations of the DLVO theory and of the RS model.

In the framework of the *DLVO theory*, the integration of Eq. (3) yields [15]:

$$\frac{d\Phi}{dx} = \sqrt{2}\kappa\left(\cosh\Phi - \cosh\Phi_m\right)^{1/2} \tag{5}$$

Φ_m is the dimensionless potential in the middle of a symmetric film, where $d\Phi/dx=0$. The integration of Eq. (5) from the film midplane ($x=0$) to the film surface ($x=h/2$) yields [15]:

$$\int_{\Phi_m}^{\Phi_s} \frac{d\Phi}{(\cosh\Phi-\cosh\Phi_m)^{1/2}} = \frac{\kappa h}{\sqrt{2}} \tag{6}$$

where $\Phi_s=\Phi|_{h/2}$ is the dimensionless surface potential. The integral in the left-hand side of Eq. (6) cannot be taken in terms of elementary functions. Finally, the electrostatic component of disjoining pressure, Π_{el}, is expressed as the difference of the osmotic pressures of the ions in the middle of the film and in the bulk of solution:

$$\frac{\Pi_{el}}{kT} = a_{2\infty}e^{\Phi_m} + (a_{1\infty}+a_{3\infty})e^{-\Phi_m} - (a_{1\infty}+a_{2\infty}+a_{3\infty}) \tag{7}$$

The electroneutrality condition, $a_{1\infty}+a_{3\infty}=a_{2\infty}$, leads to a simpler form of Eq. (7):

$$\Pi_{el} = 2kTa_{2\infty}[\cosh(\Phi_m)-1] \tag{8}$$

At a given Φ_s, Eqs. (6) and (8) give the $\Pi_{el}(h)$ dependence in a parametric form: $h=h(\Phi_m)$ and $\Pi_{el}=\Pi_{el}(\Phi_m)$ [15].

In the framework of the *RS model*, the film contains only counterions (Fig. 2b), so that the term $e^{-\Phi}$ in the right-hand side of Eq. (3) has to be omitted. Then, instead of Eq. (5), for the first integral we obtain:

$$\frac{d\Phi}{dx} = \kappa\left(e^{\Phi}-e^{\Phi_m}\right)^{1/2} \tag{9}$$

The next integration, along with the boundary condition $\Phi|_{h/2}=\Phi_s$, after some transformations yields:

$$\exp\Phi_s = \frac{\exp\Phi_m}{\cos^2\left[\frac{\kappa h}{4}\exp\left(\frac{\Phi_m}{2}\right)\right]} \tag{10}$$

Eq. (10) is an analog of Eq. (6), but this time the integral can be solved in terms of elementary functions. [The formal replacement $\Phi_s\to\Phi$ and $h/2\to x$ in Eq. (10) gives an expression for the electric potential distribution within the film, $\Phi(x)$.] Note that the right-hand side of Eq. (10) has singularities for those h values, for which the cosine in the denominator is equal to zero. For this reason, the region of physical applicability of Eq. (10) (and of the RS model) corresponds to h values, for which the argument of the cosine is between 0 and $\pi/2$:

$$0<h<\frac{2\pi}{\kappa}\exp\left(-\frac{\Phi_m}{2}\right) \tag{11}$$

In our experiments, 100 mM electrolyte is present, which leads to $\kappa^{-1}\approx 1$ nm, and the midplane potential is $\Phi_m\approx 0.7$ (see Section 4.3), so that $\exp(-\Phi_m/2)\approx 0.705$. Then, the relation (11) reduces to $0<h<4.4$ nm. (We recall that h is the thickness of the film's water core — see Fig. 2). This range of h values includes the range of thicknesses, where the hydration force is operative. For example, in our experiments, the hydration repulsion appears in the interval $0<h<3.71$ nm, irrespective of the kind of counterion (Li^+, Na^+ or Cs^+); see Section 4.1.

In the RS model, the film contains only counterions so that Eq. (7) reduces to:

$$\frac{\Pi_{el}}{kT} = a_{2\infty}e^{\Phi_m} - (a_{1\infty}+a_{2\infty}+a_{3\infty}) \tag{12}$$

Using again the electroneutrality condition, $a_{1\infty}+a_{3\infty}=a_{2\infty}$, we represent Eq. (12) in the form:

$$\Pi_{el} = kTa_{2\infty}\left(e^{\Phi_m}-2\right) \tag{13}$$

Further, having in mind that the bulk ionic strength of the solution is $I=c_{2\infty}$, and introducing the activity of the counterions in the midplane, $a_m\equiv a_{2\infty}\,e^{\Phi_m}$ we bring Eq. (13) in the form:

$$\Pi_{el} = kT(a_m-2I\gamma_{\pm}) \tag{14}$$

At a given Φ_s, Eqs. (10) and (13) determine the $\Pi_{el}(h)$ dependence (that represents the hydration force) in a parametric form: $h=h(\Phi_m)$ and $\Pi_{el}=\Pi_{el}(\Phi_m)$. As demonstrated below, the resulting theoretical $\Pi_{el}(h)$ dependence is much steeper than that predicted by the DLVO theory and can give a quantitative explanation of the experimental data at small film thicknesses.

4. Comparison of theory and experiment

4.1. Geometrical and physicochemical parameters of the system

First, let us quantify the difference between the experimental total film thickness, h_t, and the thickness of the water core, h. Insofar as we are dealing with the distributions of free counterions in an electric double layer, h is defined as the distance along the x-axis, which is accessible to the centers of the counterions. Hence, we have (see Fig. 2):

$$h_t = h + 2s, \quad s = \delta + 2r_h + 3r_i \tag{15}$$

Here, δ is the length of the surfactant's paraffin chain, r_h is the radius of the surfactant's headgroup, and r_i is the radius of the hydrated counterion. From the Tanford [66,67] formula, $\delta=0.154+0.1265n$ (nm), for $n=12$ carbon atoms in the tail, we obtain $\delta=1.672$ nm. In addition, the radius of the sulfate headgroup is $r_h=0.309$ nm [63]. The radii, r_i, of the hydrated Li^+, Na^+ and Cs^+ ions, taken from [17,68,69], are listed in Table 1. The thickness, s, of the adsorption layer at the film surface, calculated from Eq. (15), is also given in Table 1.

Fig. 3 shows the plot of the electrostatic component of disjoining pressure, $\Pi_{el}=\Pi-\Pi_{vw}$, versus the thickness of the water core, $h=h_t-2s$, calculated from Eq. (15), where h_t is the experimental total thickness (Fig. 1) and s is given in Table 1. As before, the van der Waals component of disjoining pressure is calculated from the known formula $\Pi_{vw}=-A_H/(6\pi h_t)$, where the Hamaker parameter is calculated from Eq. (5.9.3) in [70], which is based on the Lifshitz theory and takes into account the electromagnetic retardation effect.

Table 1
Values of the geometrical and physicochemical parameters of the system.

Parameter	Li^+	Na^+	Cs^+
r_i [nm]	0.382	0.358	0.329
s [nm]	3.436	3.364	3.277
$h_{t,b}$ [nm]	10.58	10.44	10.27
h_b(nm)	3.71	3.71	3.71
$\gamma_{\pm}$ for $I=0.1$ M	0.789	0.779	0.751
Φ_s^{DLVO}	5.16	3.89	3.44
$\Delta\Gamma_{2\infty}$ [μmol/m^2]	0.120	0.193	0.214
K [(mM)$^{-1}$]	2.04	2.24	2.55

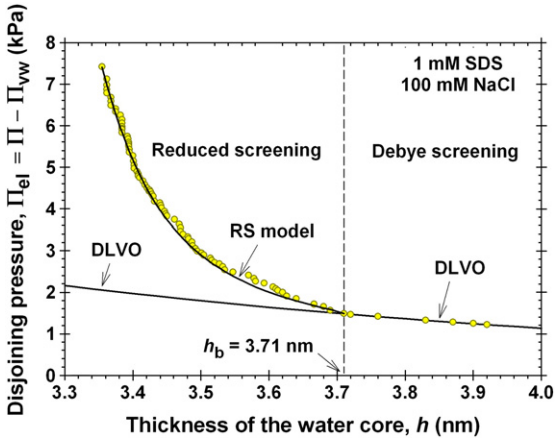

Fig. 3. Plot of the electrostatic component of disjoining pressure, $\Pi_{el} = \Pi - \Pi_{vw}$, versus the thickness of the water core of the foam film, h. The data are for a film formed from a solution of 1 mM SDS and 100 mM NaCl. In the region of Debye screening of the electric field, the data are fitted by means of the DLVO theory, Eq. (16). In the region of reduced screening, the data are fitted by means of the RS-model, Eqs. (14) and (23); details in the text.

The boundary between the regions with reduced screening and Debye screening (shown by a vertical dashed line in Fig. 3) corresponds to the value of h, at which the experimental data points deviate from the curve predicted by the DLVO theory. $h_{t,b}$ and h_b in Table 1 are the values of h_t and h, which correspond to this boundary. It is interesting, that the value $h_b = 3.71$ nm is the same for the three counterions, Li^+, Na^+ and Cs^+. This means that the difference between the three curves in Fig. 1 are dominated by the different values of s (Table 1), and more precisely, by the term $3r_i$ in Eq. (15). A possible explanation of the constancy of h_b in Table 1, could be that at this thickness the Cl^- co-ions are pressed out from the film (compare Fig. 2a and b).

The data for the activity coefficient $\gamma_\pm$ in Table 1 represent experimental values of this quantity reported in [71] for the respective electrolyte (LiCl, NaCl and CsCl) at ionic strength $I = 0.1$ M.

4.2. Processing of the data from the DLVO-branches of the experimental curves

The lower (right-hand-side) branch of the experimental curve in Fig. 3 obeys an exponential law of decay length κ^{-1} (Debye screening). To determine the surface potential, Φ_s, corresponding to this branch, we used the DLVO expression [16]:

$$\tanh^2\left(\frac{\Phi_s}{4}\right) = \frac{\Pi_{el}(h)}{64kTa_{2\infty}\exp(-\kappa h)} \tag{16}$$

The Φ_s values calculated from Eq. (16) are almost the same for all experimental points (h, Π_{el}) that belong to the DLVO branch. The obtained average values of Φ_s, denoted by Φ_s^{DLVO}, are given in Table 1. [The respective dimensional potential can be found using the fact that Φ_s is scaled with $kT/e = 25.9$ mV at 25 °C.] In the case of Na^+, we calculated independently the value of Φ_s^{DLVO} from the surface tension isotherm of SDS solutions in the presence of 100 mM NaCl in the framework of the augmented van der Waals model developed in [63]. We obtained the same value, $\Phi_s^{DLVO} = 3.89$ (see Table 1), in support of the above analysis.

The decrease of Φ_s^{DLVO} in the order $Li^+ > Na^+ > Cs^+$ indicates a reduction of the surface charge density and increase of the degree of counterion binding. This result correlates with the fact that the counterion binding energy increases from Li to Cs [72,73].

4.3. Processing of the data from the "hydration" branches of the experimental curves

First, we have to clarify what is the regime of film thinning in the framework of the RS model: fixed surface potential; fixed surface charge, or charge regulation. The equations in Section 3.2 allow us to calculate the physicochemical parameters of the system from the experimental $\Pi_{el}(h)$ data like those in Fig. 3. The midplane potential and counterion activity, Φ_m and a_m, can be calculated from the experimental Π_{el} values using Eqs. (13) and (14). Furthermore, substituting Φ_m, together with the experimental h in Eq. (10), we obtain the surface potential Φ_s. To determine the surface charge density, we have to use the electrostatic boundary condition at the film surface, which in terms of Φ reads:

$$\frac{d\Phi}{dx} = 4\pi L_B \rho_s \text{ at } x = h/2 \tag{17}$$

Here, ρ_s is the number density of the surface charges, and $L_B = e^2/(4\pi\varepsilon\varepsilon_0 kT)$ is the Bjerrum length; $L_B = 0.72$ nm for water at 25 °C. The combination of Eqs. (9), (10) and (17) yields:

$$\rho_s = \frac{\kappa}{4\pi L_B}\exp\left(\frac{\Phi_m}{2}\right)\tan\left[\frac{\kappa h}{4}\exp\left(\frac{\Phi_m}{2}\right)\right] \tag{18}$$

Substituting Φ_m and the experimental h in Eq. (18), we calculate ρ_s, which values are plotted in Fig. 4 versus h_t, together with Φ_m, Φ_s and a_m, calculated as explained above.

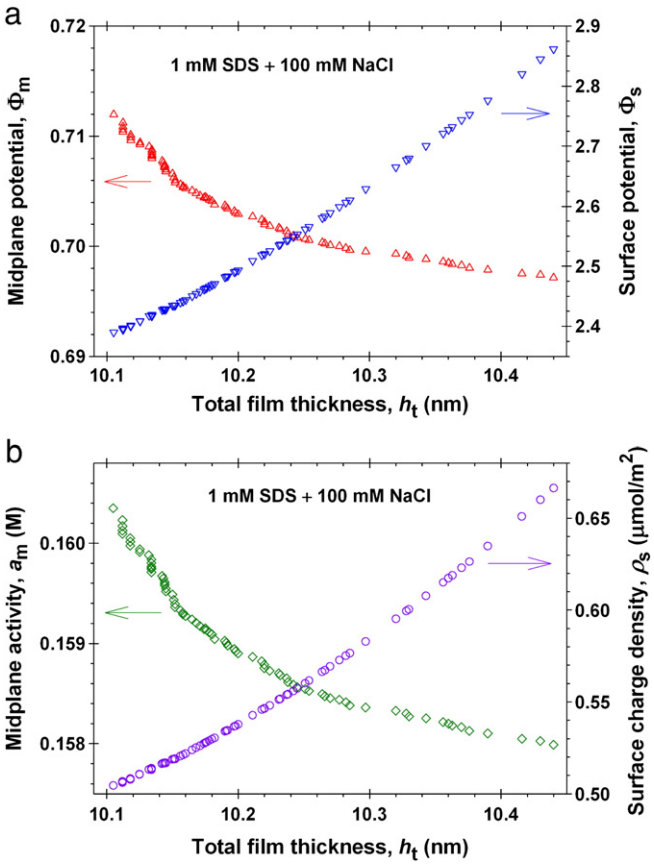

Fig. 4. Physical parameters calculated from the experimental $\Pi(h_t)$-data for the foam film from SDS + NaCl solution in Fig. 1. (a) Dimensionless midplane potential, Φ_m, and surface potential, Φ_s, calculated from Eqs. (13) and (10). (b) Midplane activity of the counterions, a_m, and number density of the surface charges, ρ_s, calculated from Eqs. (14) and (18).

Fig. 4 shows that the midplane potential and counterion activity, Φ_m and a_m, increase with the decrease of h_t, which in view of Eqs. (13) and (14) reflects the increase of Π_{el} in the same direction. From a physical viewpoint, this behavior represents the resistance of the system to the applied external pressure (the Le Chatelier–Braun principle). In contrast, the surface potential and charge, Φ_s and ρ_s, decrease with the decrease of h_t (Fig. 4). This means that the system still partially yields to the applied external pressure. The decrease of ρ_s can be interpreted as a forced condensation of counterions in the Stern layer caused by the restricted space in the interior of the thinning film. In other words, the RS model can provide a quantitative interpretation of the experimental data in the regime of *charge regulation*.

4.4. Isotherm of counterion condensation in the reduced-screening regime

The concept of attachment of counterions to a charged surface was first introduced by Stern [74] as an improvement of the electric-double-layer theory. He used a Langmuir adsorption isotherm (called also the Stern isotherm) to describe the counterion attachment. For this reason, the latter phenomenon can be termed *counterion adsorption*. Similar attachment of ions to the surfactant headgroups at the surface of micelles is called *counterion binding* [75]. An analogous binding of ions to ionized functional groups in polyelectrolytes is known as *counterion condensation* [76]. Here, we will use the terms counterion adsorption, binding, and condensation as synonyms.

The Stern isotherm was successfully applied as an element of the thermodynamic theory of adsorption of ionic surfactants in the presence of added inorganic electrolyte [61–65]. The model in [63], which excellently describes the surface-tension data for SDS, predicts that at 1 mM SDS and 100 mM NaCl the occupancy of the Stern layer is 0.75, which means that at a single air/water interface 75% of the surfactant headgroups are neutralized by bound counterions. The latter are shown by gray color in Fig. 2.

In the case of single adsorption layer of an ionic surfactant, the Stern isotherm represents a dependence of Γ_2 on a_{2s}, where Γ_2 is the adsorption of counterions in the Stern layer and $a_{2s} = a_{2\infty}\exp(\Phi_s)$ is the subsurface activity of the counterions. However, in the considered very thin films, Φ_s and a_{2s} decrease with the diminishing of the film thickness (Fig. 4a). In the considered case, the quantity that correlates with Γ_2 is the midplane activity of the counterions, $a_m = a_{2\infty}\exp(\Phi_m)$; see Fig. 4b. In such a case, the only way to formulate the Stern isotherm (the Langmuir isotherm of counterion adsorption) is in terms of Γ_2 and a_{2m}:

$$\frac{\Delta\Gamma_2}{\Delta\Gamma_{2\infty}} = \frac{K\Delta a_m}{1 + K\Delta a_m} \tag{19}$$

Here, the variations of Γ_2 and a_m are accounted with respect to their values in the beginning of the reduced-screening regime, at $h = h_b$:

$$\Delta a_m = a_m(h) - a_m(h_b) \tag{20}$$

$$\Delta\Gamma_2 = \rho_s(h_b) - \rho_s(h) \tag{21}$$

In Eq. (20), a_m can be expressed from Eq. (14): $a_m(h) = \Pi_{el}(h)/(kT) + 2I\gamma_{\pm}$. In Eq. (21), $\rho_s(h)$ is to be calculated from Eq. (18). In Eq. (19), K is an adsorption constant and $\Delta\Gamma_{2\infty}$ is the surface density of the adsorption sites that are available in the reduced-screening regime.

Fig. 5 shows the plots of $\Delta\Gamma_2$ versus Δa_m obtained from the three experimental curves in Fig. 1. As expected, the adsorption is the largest for Cs and the smallest for Li. The solid lines are the best fits by means of Eq. (19). The parameters of the model, K and $\Delta\Gamma_{2\infty}$, determined from the fits are given in Table 1. The adsorption constant K increases from Li^+ to Cs^+, which is in agreement with the expectation that the counterion binding energies increase in the same direction. The surface density of the adsorption sites, $\Delta\Gamma_{2\infty}$, is the smallest for Li^+. This could be explained with the fact that the cross-sectional area of the Li^+ ion $\pi r_i^2 = 0.46\ nm^2$ is considerably greater than that of the area per surfactant headgroup, $\pi r_h^2 = 0.30\ nm^2$. Thus, the total area occupied by the Li^+ ions at $h = h_b$ can be large enough to make inaccessible many of the surfactant headgroups considered as adsorption centers.

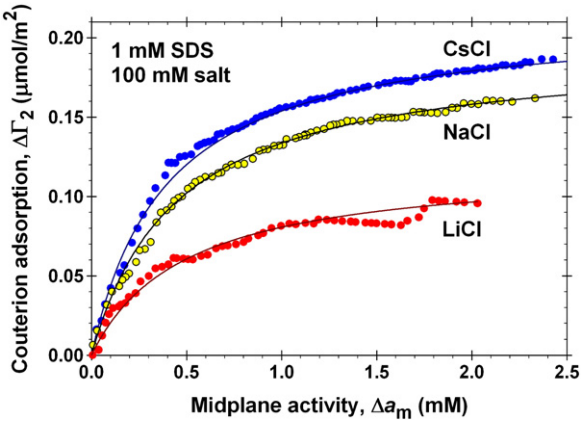

Fig. 5. Isotherms of counterion condensation in reduced-screening regime corresponding to the data in Fig. 1. $\Delta\Gamma_2 = \Gamma_2(h) - \Gamma_2(h_b) = \rho_2(h_b) - \rho_2(h)$ is calculated from Eq. (18). $\Delta a_m = a_m(h) - a_m(h_b)$ is calculated from Eq. (14). The solid lines are fits by a Langmuir isotherm, Eq. (19); the parameters of the fits, K and $\Delta\Gamma_{2\infty}$, are given in Table 1.

The fact that the curves in Fig. 5 are described by Eq. (19) with a constant K means that the energy for transfer of a counterion from the midplane to the Stern layer is independent of the film thickness. For the time being, we cannot explain this result. In fact, the whole experimental range of thicknesses where the hydration force is acting is very narrow; e.g. in Fig. 3 it is between 3.35 and 3.71 nm, i.e. within 0.36 nm. At such small distances the continuum mean-field theory is at the edge of its applicability. Additional effects, such as charge discreteness, alterations in the dielectric constant and strongly anisotropic pressure tensor, could affect the results. From this viewpoint, Eq. (19) and its agreement with the data (Fig. 5) should be considered as an empirical mean-field description of the charge regulation in the investigated very thin films.

4.5. The force vs. distance law predicted by the RS model

"Debye screening" is the regime in which $\Pi_{el}(h)$ decays exponentially with a decay length equal to the Debye length, κ^{-1}. Such are the lower branches of the experimental curves shown in Figs. 1 and 3. In contrast, in the RS model the $\Pi_{el}(h)$ dependence, determined by Eqs. (10) and (13), is not described by a simple exponential law due to the rather specific form of Eq. (10). Because the latter creates computational difficulties, for the reader convenience we briefly outline the procedure used to calculate the theoretical curves for the hydration force in Fig. 1.

Using the definitions of κ, L_B and a_m, we can represent Eq. (18) in the form:

$$\rho_s(a_m, h) = \frac{a_m^{1/2}}{(2\pi L_B)^{1/2}} \tan\left[(2\pi L_B a_m)^{1/2}\frac{h}{2}\right] \tag{22}$$

Then, in view of Eqs. (20)–(22), Eq. (19) acquires the form:

$$\frac{\rho_s\left(a_{m,b}, h_b\right) - \rho_s(a_m, h)}{\Delta\Gamma_{2\infty}} = \frac{K\left(a_m - a_{m,b}\right)}{1 + K\left(a_m - a_{m,b}\right)} \tag{23}$$

a_m is determined by solving Eq. (23) numerically for a given value of h. Finally, the obtained value of a_m is substituted in Eq. (14) to calculate Π_{el}. The input parameters are L_B; $\Delta\Gamma_{2\infty}$; K; h_b, and $a_{m,b} = \Pi_{el}(h_b)/(kT) + 2I\gamma\pm$; see Eq. (14) and Table 1. In our calculations, $\Pi_{el}(h_b)$ was taken from the experiment, at the border between the regimes of reduced and Debye screening; see Fig. 3. In the case of theoretical modeling, one can use the $\Pi_{el}(h_b)$ value predicted by the DLVO theory. The model is applicable not only to foam films, but also to any films from aqueous electrolyte solutions that are formed between two charged surfaces, including solid ones. Additional work is necessary to verify the applicability of the RS model to different systems at various electrolyte concentrations.

With the surface-force apparatus [17] and with the CP-AFM technique [34], it is possible to measure greater surface forces between solid surfaces in comparison with the MJ method [55], which is applicable to free foam films. Therefore, it is interesting to investigate the predictions of the RS model at smaller thicknesses and higher pressures. From a physical viewpoint, the decrease of h leads to two competitive effects: (i) increase of the osmotic-overlap repulsion due to the counterions confined between the two film surfaces and (ii) enhancement of the counterion condensation (Fig. 5). As shown below, each of these two tendencies may prevail depending on the parameter values.

First, let us consider the case of $\rho_s(h_b) > \Delta\Gamma_{2\infty}$. For $h \to 0$, Eq. (22) yields $\rho_s = a_m h/2$. Hence, at a finite ρ_s we have $a_m \to \infty$ for $h \to 0$. Then, Eq. (23) reduces to $[\rho_s(h_b) - a_m h/2]\ /\Delta\Gamma_{2\infty} = 1$. Expressing a_m from the latter equation and substituting it in Eq. (14), we obtain the asymptotics of Π_{el}:

$$\Pi_{el} = kT\frac{2}{h}[\rho_s(h_b) - \Delta\Gamma_{2\infty}] \text{ for } h \to 0 \tag{24}$$

In our case, the parameter values correspond to the asymptotic Eq. (24), as illustrated in Fig. 6. $\Pi_{el} \sim 1/h$ corresponds to an increase of the osmotic-overlap repulsion due to counterions confined between the two film surfaces. From a physical viewpoint, this case is realized when the excluded area per counterion in the Stern layer is greater than the area per surface charge. (In the case of foam films, this corresponds to counterions, which are bigger than the ionic-surfactant headgroups.) Then, after the Stern layer is occupied, a part of the counterions remain in the film core and give rise to the aforementioned osmotic repulsion.

Second, let us consider the case of $\rho_s(h_b) < \Delta\Gamma_{2\infty}$. For $h \to 0$, Eq. (22) yields $\rho_s \to 0$ (complete counterion condensation) at a finite a_m. Next, we formally set $\rho_s(h) = 0$ in Eq. (23), express a_m from the resulting equation, and substitute it in Eq. (14). Thus, we obtain:

$$\Pi_{el} = \frac{kT}{K}\frac{\rho_s(h_b)}{\Delta\Gamma_{2\infty} - \rho_s(h_b)} + \Pi_{el}(h_b) \text{ for } h \to 0 \tag{25}$$

Hence, in this case Π_{el} has a finite value at $h \to 0$. As already mentioned, Eq. (25) describes the asymptotic case of prevailing counterion condensation. Physically, this case can be realized when the area per surface charge is greater than the excluded area per counterion in the Stern layer, so that all counterions could condense in a monolayer.

Finally, in the special case $\rho_s(h_b) = \Delta\Gamma_{2\infty}$ the asymptotic behavior of Π_{el} is described by the expression:

$$\Pi_{el} = kT\left(\frac{2\Delta\Gamma_{2\infty}}{Kh}\right)^{1/2} \text{ for } h \to 0 \tag{26}$$

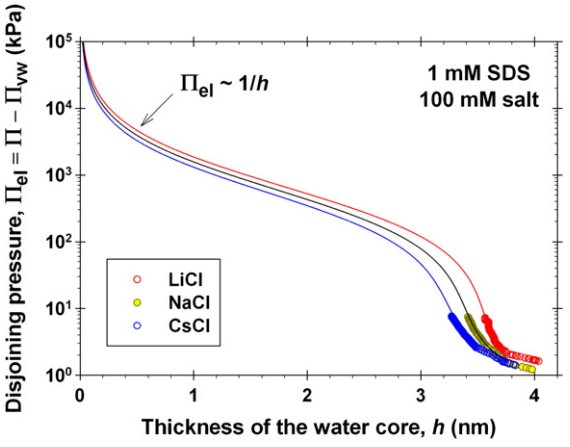

Fig. 6. Behavior of the theoretical curves for Π_{el} vs. h from Fig. 1b at smaller film thicknesses. The curves are calculated from Eqs. (14) and (23) with $\Delta\Gamma_{2\infty}$ and K from Table 1. At $h \to 0$, the electrostatic disjoining pressure is $\Pi_{el} \sim 1/h$, see Eq. (24). The data points are the same as in Fig. 1.

5. Summary and conclusions

To investigate the action of hydration force in thin films, experiments with foam films from solutions of 1 mM SDS + 100 mM electrolyte (LiCl, NaCl and CsCl) were carried out in an MJ cell. The measured dependences of disjoining pressure versus film thickness exhibit a steep increase when the thickness of the film's water core, h, becomes smaller than 3.7 nm (see Figs. 1 and 3, and Table 1). This behavior can be considered as a manifestation of the hydration force. When plotted vs. the total thickness of the foam films, h_t, the experimental curves corresponding to larger counterions are shifted toward greater thicknesses (Fig. 1). The increment of the shift is equal to six times the radius of the hydrated counterion, r_i; see Eq. (15) and the related text.

To interpret the data, a new model is proposed which assumes that at sufficiently small thicknesses all co-ions are pressed out of the film so that it contains only counterions dissociated from the ionized surface groups. Under such conditions, the screening of the electric field of the film surfaces weakens, which considerably enhances the electrostatic repulsion, Π_{el}, in comparison with that predicted by the DLVO theory. Such reduced screening of the electric field could exist only in a narrow range of film thicknesses, which practically coincides with the range where the hydration repulsion is observed; see Eq. (11) and the related text. Furthermore, it is demonstrated that in combination with a charge-regulation regime (Section 4.4), the proposed reduced-screening model of hydration force can provide a quantitative explanation of the observed strong repulsion at small separations.

The results can be important for a better understanding and control of the stability of various disperse systems (foams, emulsions, suspensions, lamellar phases, model and biological phospholipid membranes) at high electrolyte concentrations.

Acknowledgements

We thankfully acknowledge the support from the National Science Fund of Bulgaria, Grant no. DID-02-18/2009 and from COST Action D43 of ESF. The authors are grateful to Prof. Thomas Zemb for his stimulating interest in this study.

References

[1] Kruyt HR, Bungenberg de Jong HG. Zur Kenntnis der lyophilen Kolloide I. Mitteilung Allgemeine Einleitung: Das Agarsol. Kolloid Beihefte 1928;28:1–54, doi:10.1007/BF02556743.
[2] Norrish K. The swelling of montmorillonites. Discuss Faraday Soc 1954;18:120–34.
[3] van Olphen H. Interlayer forces in bentonite. Clays Clay Minerals 1954;2:418–38.
[4] Clunie JS, Goodman JF, Symons PC. Solvation forces in soap films. Nature London 1967;216:1203–4.

[5] Jordine EStA. Specific interactions which need nonequilibrium particle/particle models. J Colloid Interface Sci 1973;45:435–9.
[6] Derjaguin BV, Churaev NV. Structural component of disjoining pressure of thin layers of liquids. Croatica Chem Acta 1977;50:187–95.
[7] LeNeveu DM, Rand RP, Parsegian VA, Gingell D. Measurement and modification of forces between lecithin bilayers. Biophys J 1977;18:209–30.
[8] Lis LJ, McAlister M, Fuller N, Rand RP, Parsegian VA. Interactions between neutral phospholipid bilayer membranes. Biophys J 1982;37:657–65.
[9] Israelachvili JN, Adams GE. Measurements of forces between two mica surfaces in aqueous electrolyte solutions in the range 0–100 nm. J Chem Soc Faraday Trans 1 1978;74:975–1001.
[10] Pashley RM, Israelachvili JN. A comparison of surface forces and interfacial properties of mica in purified surfactant solutions. Colloids Surfaces 1981;2: 169–87.
[11] Pashley RM, Israelachvili J. Molecular layering of water in thin films between mica surfaces and its relation to hydration forces. J Colloid Interface Sci 1984;101: 511–22.
[12] Pashley RM. Hydration forces between mica surfaces in aqueous electrolyte solutions. J Colloid Interface Sci 1981;80:153–62.
[13] Pashley RM. DLVO and hydration forces between mica surfaces in Li^+, Na^+, K^+, and Cs^+ electrolyte solutions: a correlation of double-layer and hydration forces with surface cation exchange properties. J Colloid Interface Sci 1981;83:531–46.
[14] Pashley RM. Hydration forces between mica surfaces in electrolyte solutions. Adv Colloid Interface Sci 1982;16:57–62.
[15] Derjaguin BV, Landau LD. Theory of the stability of strongly charged lyophobic sols and of the adhesion of strongly charged particles in solutions of electrolytes. Acta Physicochim URS 1941;14:633–62.
[16] Verwey EJW, Overbeek JThG. Theory of the stability of lyophobic colloids. Amsterdam: Elsevier; 1948.
[17] Israelachvili JN. Intermolecular and surface forces. London: Academic Press; 1992.
[18] Peschel G, Belouschek P, Müller MM, Müller MR, König R. The interaction of solid surfaces in aqueous systems. Colloid Polym Sci 1982;260:444–51.
[19] Horn RG, Smith DT, Haller W. Surface forces and viscosity of water measured between silica sheets. Chem Phys Lett 1989;162:404–8.
[20] Claesson P, Carmona-Ribeiro AM, Kurihara K. Dihexadecyl phosphate monolayers: intralayer and interlayer interactions. J Phys Chem 1989;93:917–22.
[21] Petsev DN, Vekilov PG. Evidence for non-DLVO hydration interactions in solutions of the protein apoferritin. Phys Rev Lett 2000;84:1339–42.
[22] Petsev DN, Thomas BR, Yau S-T, Vekilov PG. Interactions and aggregation of apoferritin molecules in solution: effects of added electrolytes. Biophys J 2000;78: 2060–9.
[23] Valle-Delgado JJ, Molina-Bolívar JA, Galisteo-González F, Gálvez-Ruiz MJ, Feiler A, Rutland MW. Existence of hydration forces in the interaction between apoferritin molecules adsorbed on silica surfaces. Langmuir 2005;21:9544–54.
[24] Aroti A, Leontidis E, Dubios M, Zemb T. Effects of monovalent anions of the hofmeister series on DPPC lipid bilayers Part I: swelling and in-plane equations of state. Biophys J 2007;93:1580–90.
[25] Leontidis E, Aroti A, Belloni L, Dubios M, Zemb T. Effects of monovalent anions of the hofmeister series on DPPC lipid bilayers Part II: modeling the perpendicular and lateral equation-of-state. Biophys J 2007;93:1591–607.
[26] Sanfeld A, Steinchen A. Emulsions stability, from dilute to dense emulsions — role of drops deformation. Adv Colloid Interface Sci 2008;140:1–65.
[27] Kaldasch J, Senge B, Laven J. The impact of non-DLVO forces on the onset of shear thickening of concentrated electrically stabilized suspensions. Rheol Acta 2009;48:665–72.
[28] Bongrand P. Intermolecular forces. In: Bongrand P, editor. Physical basis of cell–cell adhesion. Boca Raton, FL: CRC Press; 1987. p. 1–37.
[29] Binder B, Goede A, Berndt N, Holzhütter H-G. A conceptual mathematical model of the dynamic self-organisation of distinct cellular organelles. PLoS One 2009;4: 1–12, doi:10.1371/journal.pone.0008295.
[30] Rand R, Parsegian V. Hydration forces between phospholipid bilayers. Biochim Biophys Acta 1989;988:351–76.
[31] Cevc G. Hydration force and the interfacial structure of the polar surface. J Chem Soc Faraday Trans 1991;87:2733–9.
[32] Leikin S, Parsegian VA, Rau DC, Rand RP. Hydration forces. Annu Rev Phys Chem 1993;44:369–95.
[33] Israelachvili J, Wennerström H. Role of hydration and water structure in biological and colloidal interactions. Nature 1996;379:219–25.
[34] Butt H-J, Capella B, Kappl M. Force measurements with the atomic force microscope: technique, interpretation and applications. Surface Sci Reports 2005;59:1–152.
[35] Marčelja S, Radić N. Repulsion of interfaces due to boundary water. Chem Phys Lett 1976;42:129–30.
[36] Besseling NAM. Theory of hydration forces between surfaces. Langmuir 1997;13: 2113–22.
[37] Forsman J, Woodward CE, Jönsson B. The origins of hydration forces: Monte Carlo simulations and density functional theory. Langmuir 1997;13:5459–64.
[38] Jönsson B, Wennerström H. Image-charge forces in phospholipid bilayer systems. J Chem Soc Faraday Trans 2 1983;79:19–35.
[39] Kjellander R. On the image-charge model for the hydration force. J Chem Soc Faraday Trans 2 1984;80:1323–48.
[40] Bratko D, Jönsson B. Electrical double layer interactions with image charges. Chem Phys Lett 1986;128:449–54.
[41] Trokhymchuk A, Henderson D, Wasan DT. A molecular theory of the hydration force in an electrolyte solution. J Colloid Interface Sci 1999;210:320–31.
[42] Simon SA, McIntosh TJ. Magnitude of the solvation pressure depends on dipole potential. Proc Natl Acad Sci USA 1989;86:9263–7.
[43] Richmond P. Electrical forces between particles with arbitrary fixed surface charge distributions in ionic solution. J Chem Soc Faraday Trans 2 1974;70:1066–73.
[44] Dzhavakhidze PG, Kornyshev AA, Levadny VG. The structure of the interface in the solvent-mediated interaction of dipolar surfaces. Nuovo Cimento 1988;10D:627–53.
[45] Kornyshev AA, Leikin S. Fluctuation theory of hydration forces: the dramatic effects of inhomogeneous boundary conditions. Phys Rev A 1989;40:6431–7.
[46] Leikin S, Kornyshev AA. Theory of hydration forces. Nonlocal electrostatic interaction of neutral surfaces. J Chem Phys 1990;92:6890–8.
[47] Attard P, Patey GN. Continuum electrostatic interactions between planar lattices of dipoles and the possible relevance to the hydration force. Phys Rev A 1991;43:2953–62.
[48] Henderson D, Lozada-Cassou M. A simple theory for the force between spheres immersed in a fluid. J Colloid Interface Sci 1986;114:180–3.
[49] Henderson D, Lozada-Cassou M. Note: does dielectric saturation provide a plausible explanation of the hydration solvation force? J Colloid Interface Sci 1994;162:508–9.
[50] Basu S, Sharma MM. Effect of dielectric saturation on disjoining pressure in thin films of aqueous electrolytes. J Colloid Interface Sci 1994;165:355–66.
[51] Paunov VN, Dimova RI, Kralchevsky PA, Broze G, Mehreteab A. The hydration repulsion between charged surfaces as an interplay of volume exclusion and dielectric saturation effects. J Colloid Interface Sci 1996;182:239–48.
[52] Paunov VN, Binks BP. Analytical expression for the electrostatic disjoining pressure taking into account the excluded volume of the hydrated ions between charged interfaces in electrolyte. Langmuir 1999;15:2015–21.
[53] Israelachvili JN, Wennerström H. Entropic forces between amphiphilic surfaces in liquids. J Phys Chem 1992;96:520–31.
[54] Brzozowska AM, Spruijt E, de Keizer A, Cohen Stuart MA, Norde W. On the stability of the polymer brushes formed by adsorption of ionomer complexes on hydrophilic and hydrophobic surfaces. J Colloid Interface Sci 2011;353:380–91.
[55] Mysels KJ, Jones MN. Direct measurement of the variation of double-layer repulsion with distance. Discuss Faraday Soc 1966;42:42–50.
[56] Schelero N, Hedicke G, Linse P, von Klitzing R. Effects of counterions and co-ions on foam films stabilized by anionic dodecyl sulfate. J Phys Chem B 2010;114:15523–9.
[57] Sheludko A. Thin liquid films. Adv Colloid Interface Sci 1967;1:391–464.
[58] Bergeron V, Radke CJ. Equilibrium measurements of oscillatory disjoining pressures in aqueous foam films. Langmuir 1992;8:3020–6.
[59] Dimitrova TD, Leal-Calderon F, Gurkov TD, Campbell B. Disjoining pressure vs thickness isotherms of thin emulsion films stabilized by proteins. Langmuir 2001;17: 8069–77.
[60] Kirkwood JG, Oppenheim I. Chemical thermodynamics. New York: McGraw-Hill; 1961.
[61] Kralchevsky PA, Danov KD, Broze G, Mehreteab A. Thermodynamics of ionic surfactant adsorption with account for the counterion binding: effect of salts of various valency. Langmuir 1999;15:2351–65.
[62] Kolev VL, Danov KD, Kralchevsky PA, Broze G, Mehreteab A. Comparison of the van der Waals and Frumkin adsorption isotherms for sodium dodecyl sulfate at various salt concentrations. Langmuir 2002;18:9106–9.
[63] Kralchevsky PA, Danov KD, Kolev VL, Broze G, Mehreteab A. Effect of nonionic admixtures on the adsorption of ionic surfactants at fluid interfaces. 1. Sodium dodecyl sulfate and dodecanol. Langmuir 2003;19:5004–18.
[64] Valkovska DS, Shearman GC, Bain CD, Darton RC, Eastoe J. Adsorption of ionic surfactants at an expanding air–water interface. Langmuir 2004;20:4436–45.
[65] Kralchevsky PA, Danov KD, Denkov ND. Chemical physics of colloid systems and interfaces. In: Birdi KS, editor. Handbook of surface and colloid chemistry. Boca Raton, FL: CRC Press; 2008. p. 197–377.
[66] Tanford C. The hydrophobic effect. The formation of micelles and biological membranes. New York: Wiley; 1980.
[67] Hiemenz PC, Rajagopalan R. Principles of colloid and surface chemistry. New York: Marcel Dekker; 1997.
[68] Cotton FA, Wilkinson G. Advanced inorganic chemistry. New York: Wiley; 1983.
[69] Pandey S, Bagwe RP, Shah DO. Effect of counterions on surface and foaming properties of dodecyl sulfate. J Colloid Interface Sci 2003;267:160–6.
[70] Russel WB, Saville DA, Schowalter WR. Colloidal dispersions. Cambridge: Cambridge University Press; 1989.
[71] Hamer WJ, Wu Y-C. Osmotic coefficients and mean activity coefficients of univalent electrolytes in water at 25 °C. J Phys Chem Ref Data 1972;1:1047–99.
[72] Lu JR, Marrocco A, Su TJ, Thomas RK, Penfold J. Adsorption of dodecyl sulfate surfactants with monovalent metal counterions at the air–water interface studied by neutron reflection and surface tension. J Colloid Interface Sci 1993;158:303–16.
[73] Karakashev S, Tsekov R, Manev E. Adsorption of alkali dodecyl sulfates on air/water surface. Langmuir 2001;17:5403–5.
[74] Stern O. Zur Theorie der Elektrolytischen Doppelschicht. Z Elektrochem 1924;30: 508–16.
[75] Rathman JF, Scamehorn JF. Counterion binding on mixed micelles. J Phys Chem 1984;88:5807–16.
[76] Oosawa F. Polyelectrolytes. New York: M. Dekker; 1971.